C. R. Physique 17 (2016) 1018–1026

Contents lists available at ScienceDirect

Comptes Rendus Physique

www.sciencedirect.com

Probing matter with electromagnetic waves / Sonder la matière par les ondes électromagnétiques

Microwave imaging of magnetohydrodynamic instabilities in fusion plasma

Imagerie micro-ondes dans les plasmas de fusion magnétique pour visualiser les instabilités magnéto-hydrodynamiques

Roland Sabot [a,*], Didier Elbèze [a], Woochang Lee [b], Yoonbum Nam [c], Hyeon Park [b], Junsong Shen [a,d], Gunsu Yun [c], Minjun Choi [c], Jean-Claude Giacalone [a], Timothée Nicolas [a], Christine Bottereau [a], Frédéric Clairet [a], Philippe Lotte [a], Diego Molina [a]

[a] *CEA, IRFM, 13108 Saint-Paul-lez-Durance, France*
[b] *Ulsan National Institute of Science and Technology, Ulsan, Republic of Korea*
[c] *Pohang University of Science and Technology, Pohang, Republic of Korea*
[d] *ASIPP, 230031 Hefei, People's Republic of China*

ARTICLE INFO

Article history:
Available online 12 August 2016

Keywords:
Fusion plasma diagnostic
Radiometry
Reflectometry
MHD

Mots-clés :
Diagnostic pour les plasmas de fusion
Radiométrie
Réflectométrie
MHD

ABSTRACT

Microwave imaging diagnostics are extremely useful for observing magnetohydrodynamic (MHD) instabilities in magnetic fusion plasmas. Two imaging diagnostics will be available on the WEST tokamak. A method was developed to reconstruct electron density maps from electron density profiles measured by ultrafast reflectometry, a technique based on FM-CW radar principle. It relies on plasma rotation to perform 2D reconstruction. An Electron Cyclotron Emission Imaging (ECEI) diagnostic will image directly the temperature fluctuations. It will be equivalent to 24 stacked vertically radiometers, each probing a spot of few centimetres. These two complementary techniques will contribute to the validation of MHD models.

RÉSUMÉ

Les instruments d'imagerie micro-ondes se sont révélés extrêmement utiles pour analyser les instabilités magnétohydrodynamiques (MHD) dans les plasmas de fusion magnétique. Deux diagnostics d'imagerie seront disponibles sur le tokamak WEST. Une méthode a été développée pour reconstruire une image bidimensionnelle de la densité du plasma à partir des profils de densité mesurés par réflectométrie ultrarapide, une technique basée sur le principe du radar FM-CW. Un diagnostic de radiométrie fournira une image des fluctuations de température à partir de l'émission à la fréquence cyclotronique électronique (ECE). Ces

* Corresponding author.
E-mail address: roland.sabot@cea.fr (R. Sabot).

http://dx.doi.org/10.1016/j.crhy.2016.07.021

deux systèmes seront complémentaires et contribueront à valider les modèles numériques de MHD.

1. Introduction

The goal of nuclear fusion research is to demonstrate the scientific and technical feasibility of nuclear fusion as a clean energy source. Deuterium and tritium plasma must be heated to temperature exceeding 100 million degrees (10 times the temperature in the sun core) to produce fusion reactions. The tokamak approach is currently the most promising method path available for achieving the conditions required for producing controlled fusion power.

In a tokamak, the plasma is confined by strong magnetic fields. These fields generate a set of nested magnetic tori called magnetic surfaces, which isolate the core where thermonuclear conditions are reached from the colder edge in interaction with the vacuum vessel [1]. Magnetohydrodynamic (MHD) instabilities can perturb this nested magnetic configuration, leading to deleterious effects from performance reductions to abrupt terminations of the discharge. High-performance numeric models are being developed to simulate MHD instabilities. Extrapolation to ITER is also crucial. ITER, under construction in the south of France by seven international partners, will be the first fusion experiment where the plasma will be self-heated by the energetic alpha particles generated by fusion reactions. Study and control of burning plasmas is a major objective as these energetic particles can excite various MHD instabilities [2].

To validate these MHD codes, simulations must be compared to experiments using accurate and sensitive measurements. Nowadays, microwave imaging instruments offering a 2-D visualisation phenomena inside the plasma are essential and they have already been developed on many fusion machines [3–6]. They have proven extremely useful for understanding the physics of MHD instabilities as they give direct visualisation of the spatial structures and their temporal evolution. The first sawtooth crash images from Electron Cyclotron Emission Imaging (ECEI) were a major step forward in the understanding of this phenomenon, which causes periodic reorganisation of the plasma core equilibrium. The unambiguous picture presented by ECEI revealed a highly localized reconnection event [7,8]. ECEI characterized also for the first time the electron temperature structure associated with fast particle-induced MHD modes [5]. The poloidal structure and dynamics of Elms, an MHD mode that develops at the plasma edge was visualized by ECEI [9]. Elms (Edge Localized Modes) are quasi-periodic relaxation phenomena that induce a collapse of the temperature and particle edge profiles in high confinement regimes (H-mode). In ITER, energy expulsion during Elms could damage the plasma-facing components and in particular, the divertor plates.

On WEST, two microwave diagnostics will provide images of MHD instabilities. The density perturbations induced by MHD instabilities will be imaged using ultrafast reflectometry. An ECEI radiometer will detect electron temperature fluctuations. WEST (Tungsten (W) Environment (E) Steady-state (S) Tokamak (T)) is an upgrade of Tore Supra tokamak that aims to test critical components for ITER such as divertor plates during pulse lasting up to 1000 seconds. A magnetic configuration closer to ITER will be obtained by installing poloidal field coils in the vacuum vessel [10]. The first plasma in WEST is expected end of 2016.

The paper is organized as follows. The technique to reconstruct 2-D images from ultra-fast reflectometry measurements of density profiles is first presented. The next part focuses on the development of an ECEI diagnostic under Korean–French collaboration. Access constraint and long-pulse operations on WEST impose specific implantation compared to existing ECEI diagnostics. The conclusion underlines the synergy between both techniques for MHD understanding.

2. 2D reconstruction of electron density

2.1. Reflectometry principle

Derived from radar principle, reflectometry measures the electron density in plasma. It was first applied to the ionosphere following radar development in the 1930s. Measurements in magnetic fusion date back to the 1980s [11]. The wave frequency is chosen in such a way that the wave propagates in the outer part of the plasma until it reaches a cut-off layer where it is reflected. As the wave is launched perpendicularly to the plasma magnetic field $\mathbf{B}_t$, two polarisations can propagate. In ordinary-mode (O-mode, $\mathbf{E}/\!/\mathbf{B}_t$, $\mathbf{E}$ the wave electric field), the cut-off pulsation depends only on the local electron density n_e:

$$\omega_p = \left(\frac{n_e e^2}{\varepsilon_0 m_e}\right)^{0.5} \tag{1}$$

In extraordinary polarisation (X-mode) for $\mathbf{E} \perp \mathbf{B}_t$, the cut-off frequency depends also on the magnetic field, and there are two cut-off pulsations named upper ω_R:

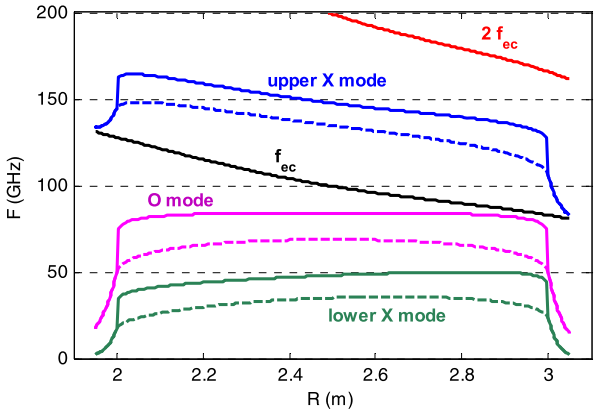

Fig. 1. Radial profiles of electron cyclotron, X-mode and O-mode cut-off frequencies in WEST for two density profiles $n_e(\rho) = (n_0 - n_a)(1-\rho^2)^\alpha + n_a$: a high central density ($n_0 = 9 \cdot 10^{19}$ m^{-3}) and flat profile ($\alpha = 0.1$) case (plain lines), a moderate central density ($n_0 = 6 \cdot 10^{19}$ m^{-3}) and stronger peaking ($\alpha = 0.5$). Both profiles have the same edge density, $n_a = 3 \cdot 10^{19}$ m^{-3}.

$$\omega_R = \frac{1}{2}\left(\sqrt{4\omega_p^2 + \omega_{ec}^2} + \omega_{ec}\right) \tag{2}$$

and lower cut-off ω_L:

$$\omega_L = \frac{1}{2}\left(\sqrt{4\omega_p^2 + \omega_{ec}^2} - \omega_{ec}\right) \tag{3}$$

where $\omega_{ec} = \frac{qB_t}{m_e}$ is the electron cyclotron pulsation.

Fig. 1 shows the radial profiles of the different cut-off frequencies in WEST (major radius $R_0 = 2.5$ m, minor radius $a = 0.5$ m) at the nominal magnetic field ($B_t = 3.8$ T in the centre). In upper X-mode, a reflectometer on the outer side can probe almost the whole plasma from the edge to the centre and the inner side. O-mode is restricted to the edge pedestal in case of flat density profiles. Lower X-mode will be used in ITER to probe plasma core from the inner side. Absorption at the second EC harmonic limits the accessibility in high-density discharges.

Reflectometry measures the phase φ_p due to the round trip inside the plasma between the plasma edge at $x = 0$ and the reflecting layer x_{co}:

$$\varphi_p = 2\frac{2\pi F}{c}\int_{x=0}^{r_{co}} N(r, F, t)\mathrm{d}r - \frac{\pi}{2} \tag{4}$$

where N is the refractive index. N decreases from 1 at the edge (vacuum) to 0 at the cut-off layer.

Reflectometry can measure the electron density profile or probe plasma turbulence. Sweeping the frequency source F is the usual method to measure the density profiles. Increasing the frequency moves the reflecting layer further inside the plasma. The position of the reflecting layer x_{co} is recovered from the phase measurement using an inversion algorithm. In O-mode, this inversion can be analytic, Abel-like inversion, but it requires phase measurements down to $F \sim 0$ [12]. In X-mode, the inversion relies on an iterative algorithm [13]: a density profile from the edge to $x_{co}(F)$ is used to recover the reflecting layer position $x_{co}(F + \delta F)$ at the probing frequency $F + \delta F$.

To minimize the disturbance due to plasma turbulence, the profile must be measured in a time comparable to the turbulence characteristic time [14]. The plasma is then frozen during the measurement as for pictures taken with a fast shutter time.

2.2. Ultra-fast profile reflectometers on Tore Supra

To achieve short-duration measurements, an original microwave setup was developed for Tore Supra tokamaks. The key element is a single sideband modulator [15]. The set-up uses a single microwave source together with a heterodyne detection as the SSBM shifts the probing frequency. Frequency multipliers raise the frequency to the desired band. The phase and amplitude of the reflected signal are measured after filtering and amplification with I/Q detection, see Fig. 2. The voltage-controlled oscillator being very agile (slew rate up to 80 GHz/s), the sweeping time is mostly limited by the capabilities of the detection system.

Three profiles reflectometers, covering the range from 50 to 155 GHz, are installed on Tore Supra. They provide density measurements in the upper X-mode from the plasma edge to the centre and the inner side.

Last improvements have reduced the profile measurement time down to few µs [16] for the edge reflectometer, which is made of two systems swept simultaneously. This duration represent a tenth to a half of the turbulence characteristic time.

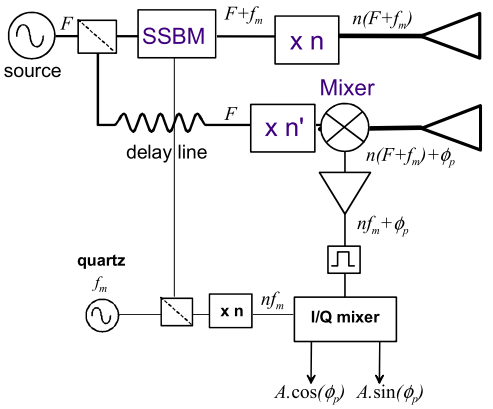

Fig. 2. Microwave set-up of Tore Supra reflectometer.

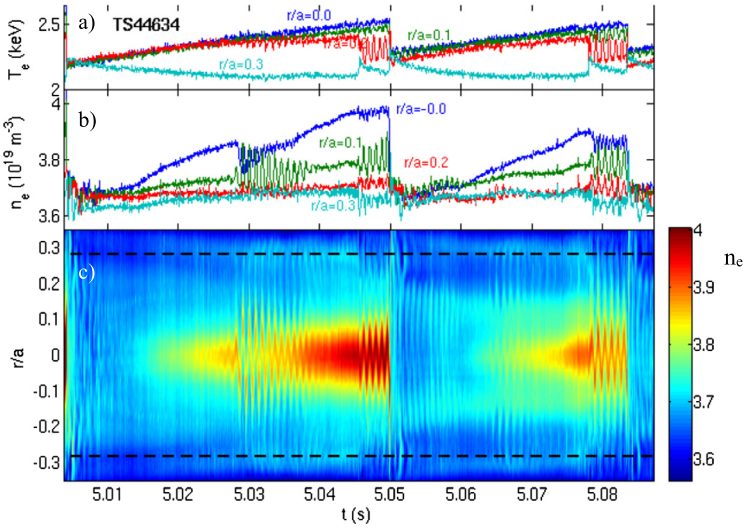

Fig. 3. The temperature a) and density evolution b) at different radii ($\rho = r/a = 0$, 0.1, 0.2 and 0.3 on low field side) during two sawteeth (TS44634, $B = 3.8$ T, $I_p = 1.2$ MA). The density evolution inside the plasma core ($r/a = -0.35$ to $r/a = 0.35$) is shown in c). The dotted line indicates the position of temperature-inversion radius.

It is one to three orders of magnitude shorter than the evolution time of large-scale density fluctuations. To achieve this improvement, the acquisition system was upgraded with sampling frequency at 2 GS/s with 10 bit vertical resolution.

The core reflectometer can also operate in fixed frequency steps to measure density fluctuations due to plasma turbulence [17]. Profiles were measured in 20 to 50 μs depending on the plasma parameters until 2012 when Tore Supra entered a long shutdown for WEST upgrade. To initialize the density profile reconstruction, this reflectometer relies on edge profile measurements from the edge reflectometer system or other density diagnostics such as interferometry [18]. For WEST restart, this reflectometer is being upgraded to perform profile measurements in a few microseconds.

2.3. 2D reconstruction of the core density during ohmic sawteeth

In a tokamak, the temperature in the plasma centre relaxes periodically. These relaxations are caused by a MHD mode that develops on a particular magnetic surface. This surface corresponds to the inversion radius, i.e. the radius where the temperature evolution during the sawtooth crash cancels. Just before the crash, density ($\delta n_e \sim 10^{18}$ m^{-3}) and temperature ($\delta T_e \sim 0.2$ keV) oscillations are detected as the plasma centre is pushed away of the magnetic axis [1] (see Fig. 3).

The precision on the density profile is sufficient to detect also density oscillations at mid-period around $r/a = 0.1$ and weaker perturbations (<1%) after the crash. These perturbations can be observed from $r/a = 0.2$ to the centre during several milliseconds.

As the plasma rotates poloidally around the magnetic axis, a 2-D image can be reconstructed to get an image of the density perturbations during a sawtooth in a vertical section. Instead of moving the detector around the probed body as in MRI (Magnetic Resonance Imaging), the detector position is fixed and the plasma spins in front of the detector. This

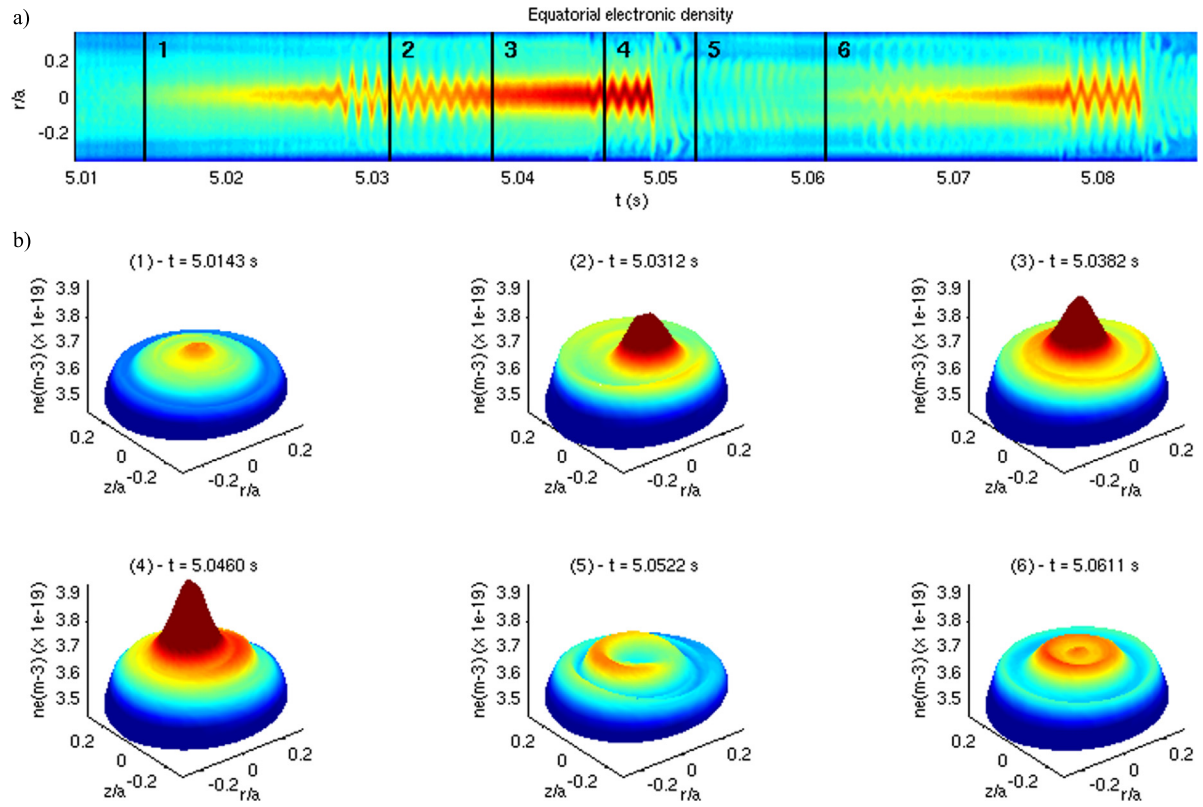

Fig. 4. 2-D image of density at 6 times during two consecutive sawteeth (b). Times are shown by vertical lines on the contour view of density profile (a). The same colour bar is used for the 2-D images and the contour view.

technique was first applied to soft-X rays tomography [19] and to ECE [20–22]. Reflectometry offers the advantages of a local measurement combined with very good radial resolution (a few millimetres) and high sensitivity ($<1\%$).

Assuming a rigid body rotation at ω_θ, a density profile measurement done at $t = t_\mathrm{i}$ in the equatorial plane ($\theta = 0$) gives also the density profile at an angle $\theta_\mathrm{i} = \omega_\theta(t_0 - t_\mathrm{i})$. However, as plasma is not stationary, one must take into account the evolution of the density profile to perform reconstructions at the same time for all poloidal angles. To correct this evolution, the density $n_\mathrm{e}(\theta_\mathrm{i}, t_0, \rho)$ at $t = t_0$, at the poloidal angle θ_i and the normalized radius ρ is obtained by linear interpolation between backward measurement made at $t = t_0 - \theta/\omega$ and forward measurement. On Tore Supra, the density profile is measured on both side of the magnetic axis, so the forward measurement corresponds to the measurement made half turn later at $t = t_0 + (\pi - \theta)/\omega_\theta$:

$$n_\mathrm{e}(\theta_\mathrm{i}, t_0, \rho) = \frac{(\pi - \theta_\mathrm{i}) \cdot n_\mathrm{e}(0, t_0 - \theta_\mathrm{i}/\omega_\theta, \rho) + \theta_\mathrm{i} \cdot n_\mathrm{e}(0, t_0 + (\pi - \theta_\mathrm{i})/\omega_\theta, \rho)}{\pi} \tag{5}$$

This technique requires fast profile measurements: the duration of the measurement must be much shorter than the plasma rotation period, which should also be much shorter than the characteristic time of the instability. For the image shown in Fig. 4, the profiles were measured in 45 µs with a dead time of 5 µs between two profiles. The rotation duration being around 900 µs (1.1 kHz), roughly 18 profiles were measured per rotation period ensuring a good angular sampling ($\Delta\theta \sim 20°$). In this discharge, the sawtooth period lasted around 40 ms, 4440 density profiles were measured consecutively in 222 ms covering five sawtooth periods.

In the ohmic shot shown in Fig. 3, the density perturbations at various radii exhibit an opposite parity between the inner ($r/a < 0$) and outer side, as expected for a mode associated with a sawtooth. Their frequency is 1.1 kHz and does not vary much during the sawtooth. Inside the inversion radius, this mode frequency is also constant along the radius, validating the assumption of rigid body rotation. Fig. 4 shows the tomography reconstruction at six different times during the two sawteeth shown in Fig. 3.

In ohmic shots, the density profile exhibits a narrow peak around the magnetic axis surrounded by a flat ring, looking like a Mexican hat [23], whereas the temperature profile is more dome-like around the centre without any flattening around the inversion radius. This narrow density peaking is caused by an inward particle pinch and a reduced particle diffusion [24].

The crescent and ring structures that appear after the sawtooth crash (time slices 5 and 6) were recovered with the XTOR-2F code [25]. During the sawtooth crash, the magnetic surfaces are reconnected and the dense hot core is expulsed outside the core. This expulsed density is then poloidal homogenised by poloidal flows to form an external ring. These flows

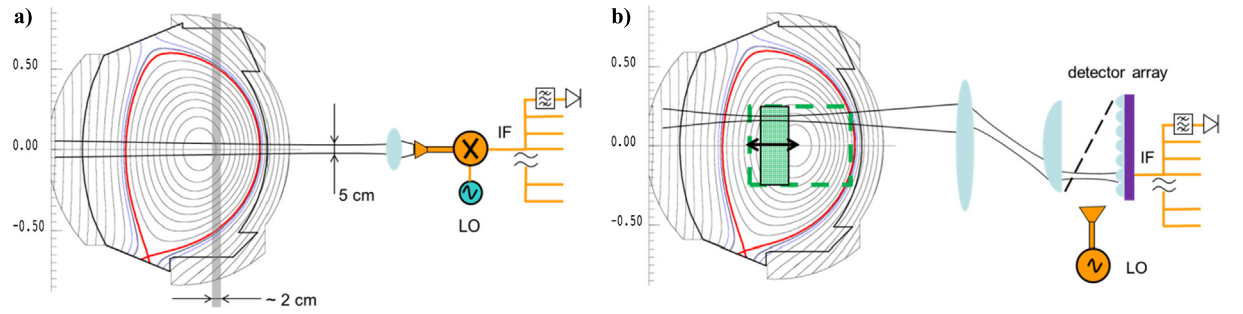

Fig. 5. Schematic diagram illustrating the principles of WEST 1D ECE radiometer (a) and ECEI diagnostic (b).

also re-inject a fraction of the expulsed density inside the core in a crescent shape structure, which is later homogenised in a poloidal manner in a more internal ring. These structures are not observed on the temperature because the latter follows the magnetic surface reconnection while the density is transported by poloidal flows, the energy transport along the field lines being much faster than particle transport. The physical model implemented in the XTOR-2F code is fully toroidal and non-linear; it includes anisotropic thermal transport, resistivity, and viscosity as well as diamagnetic drifts [26].

3. ECEI diagnostics

3.1. Principles of ECE diagnostics

In a magnetic confined plasma, charged particles gyrate around the magnetic field lines and, as a consequence, emit electromagnetic radiation at the cyclotron frequency and its harmonic [1,27]. For electrons, the cyclotron frequency f_{ece} is 28 GHz for $B = 1$ T. The radiation is anisotropically emitted and is polarised. For $\mathbf{k} \perp \mathbf{B_t}$, it is linearly polarised and occurs in both the O-mode ($\mathbf{E} // \mathbf{B_t}$) and X-mode ($\mathbf{E} \perp \mathbf{B_t}$) polarisation directions. The core of the magnetic fusion device is optically thick for the first and second harmonics of ECE radiation. A local thermodynamic equilibrium is then reached and the ECE intensity approaches the blackbody level. The thermal radiation of blackbody at few Kelvin would peak in the ECE frequency range (50–200 GHz). Indeed, the cosmic microwave background (CMB) that fits the radiation spectrum of blackbody at 2.73 K peaks around 200 GHz. As such temperatures are seven orders of magnitude lower that the plasma temperature, the low-frequency limit (Rayleigh–Jeans law) applies. The ECE intensity is thus proportional to the local electron temperature $T_e(R)$:

$$\mathrm{I}(\omega) = \frac{\omega^2 T_e(R)}{8\pi^3 c^2} \tag{6}$$

In a tokamak, the magnetic field varies in toroidal geometry monotonically as $1/R$ along the major radius R, resulting in an ECE spectrum which is a broad continuum. The emission intensity can be measured by a band-filtering heterodyne radiometer along a line of sight to reconstruct the electron temperature profiles [28]. Various effects such as Doppler broadening, relativistic corrections reduce the radial resolution of the diagnostic by about 1–3 cm. The spatial resolution of such a system in the transverse direction is limited by the divergence of the microwave beam pattern of the antenna, typically about 2–5 cm, depending on the plasma distance and frequency range (see Fig. 5a).

3.2. ECEI principles

2D images of electron temperature were first obtained using plasma rotation [20]. ECEI diagnostics were developed in the 1990s [29]. The single antenna of a classic 1D ECE is replaced by an array of antennas equivalent to several radiometers stacked vertically. Using large diameter optics and refocusing elements, the beam waist into the plasma can be decreased by about 1–2 cm and the radial resolution can reach 0.5–1 cm. The localisation is determined by the local oscillator (LO) frequency, the optics move the focus to the probing area. ECEI diagnostics give 2-D images of the temperature fluctuations with typically 8 (radial) pixels by 16 to 24 (vertical) pixels. The evolution of MHD mode structures are monitored with a time resolution around a few microseconds (see Fig. 5b).

3.3. ECEI implantation on WEST

For the WEST project, an ECEI diagnostic is being developed in collaboration with the Ulsan National Institute of Science and Technology (UNIST) and the Pohang University of Science and Technology (POSTECH). The diagnostic will operate in the O-mode polarisation as the nominal magnetic field in WEST is high ($B = 3.7$ T). Operating in the band 85–113 GHz, the diagnostic will probe the plasma from the core to the edge on the outer side (from $R = 2.3$ to $R = 3$ m) at eight frequencies. The IF bandwith will be 4.5 GHz for the 600 MHz channel spacing and 7.2 GHz for the 900 MHz channel

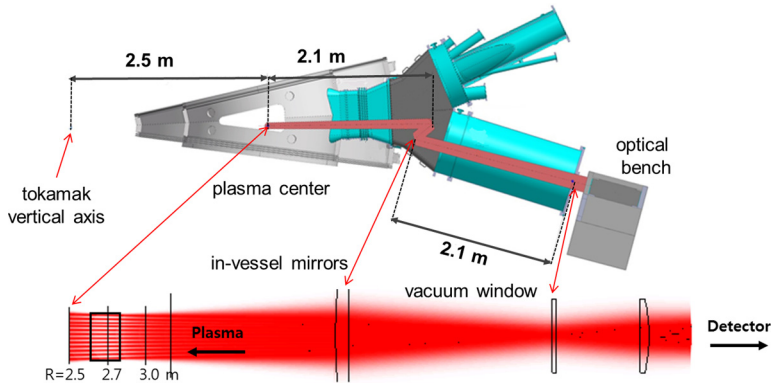

Fig. 6. Top: implantation of the ECEI beam path. Bottom: beam path with 12 beamlets (vertical view). The plasma centre is at $R = 2{,}5$ m, plasma edge at $R \leq 3$ m. The in-vessel mirrors ($\sim 20 \times 70$ cm) focus the beam near the vacuum window. Behind the window, a lens will focus the beam toward the detector arrays.

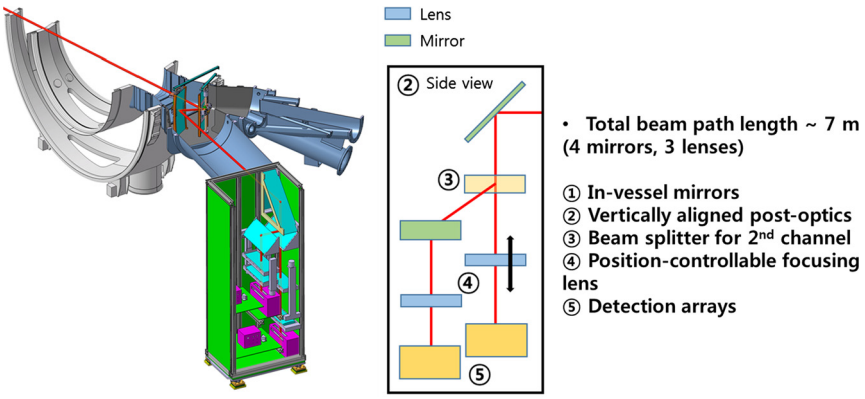

Fig. 7. Implantation in WEST of ECEI in-vessel mirrors and optical bench.

spacing. The diagnostic will have 24 vertical channels to provide 8×24 pixel images of electron temperature fluctuations. A second channel, operating in the 100–130 GHz band, will later be installed to cover the inner side ($R = 2$ to $R = 2.6$ m), allowing some overlapping with the outer system.

The diagnostic will view the plasma through the port dedicated to man access, as it is the only port where the large ECEI optics can be implemented. However, due to a man access tube, the vacuum window will be more than 5 m away from the plasma. To focalise and redirect the microwave beam, two metallic mirrors (0.2 m $\times$ 0.7 m) will be installed in the access tube 2 m away from the plasma [30], see Fig. 6. Heated by plasma radiations, the first mirror would reach 400 °C at the end of a 1000-s discharge. However, thermal expansions remain small and the optical quality of the microwave beam is not affected. Water cooling of the first mirror is thus not necessary.

Existing ECEI diagnostics are closer to the plasma and in straight view of the plasma. Composite lens outside the vacuum vessel are used, but thermal heating is not a critical issue. WEST ECEI will be the first ECEI diagnostic to be in indirect view of the plasma and to have metallic mirrors inside the vacuum vessel, a configuration that prefigure the constraints to implement ECEI diagnostic on an ITER size device.

The optical bench will be installed just behind the access tube to minimize the beam path length. Due to the limited space (1 m $\times$ 1 m) between the access tube and the access lobby, the optical bench will be vertical (Fig. 7). A lens will first refocus the beam to the detectors. A 45° mirror will reflect the beam downward. Dichroic plates will reject image frequencies. A position-controllable lens will allow one to move the focus of the beam in plasma. The probing band is set by the tuning of the LO frequency. A second detection system will later be installed to probe simultaneously another area.

The detection system is made of two rows of 12 minilenses. The rows are placed perpendicularly with a semi-reflecting plate at 45° to relax the vertical spacing constraint. This beamsplitter redirects also the LO beam to the detector rows. Each minilens beams the ECE and LO signals on a Schottky diode for heterodyne detection (Fig. 8).

Each mixer IF signal is split in eight parts corresponding to the eight probing radius. A second frequency down conversion is performed before measurement of the signal amplitude (Fig. 8). Two sets of secondary local oscillators can be chosen for either a good radial resolution ($\Delta R \sim 1.5$ cm) corresponding to a frequency channel separation of $\Delta F = 600$ MHz or a wider radial sampling ($\Delta R \sim 2.2$ cm and $\Delta F = 900$ MHz) to cover a wider probing zone (see Fig. 9).

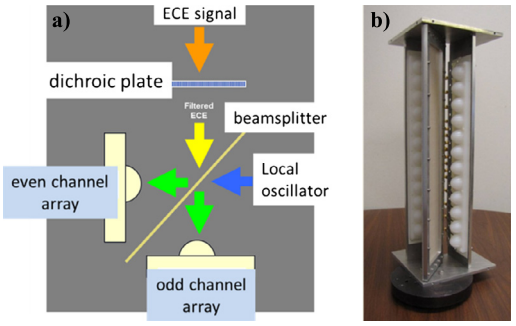

Fig. 8. a) Principe of the detection array. b) Minilens and beamsplitter.

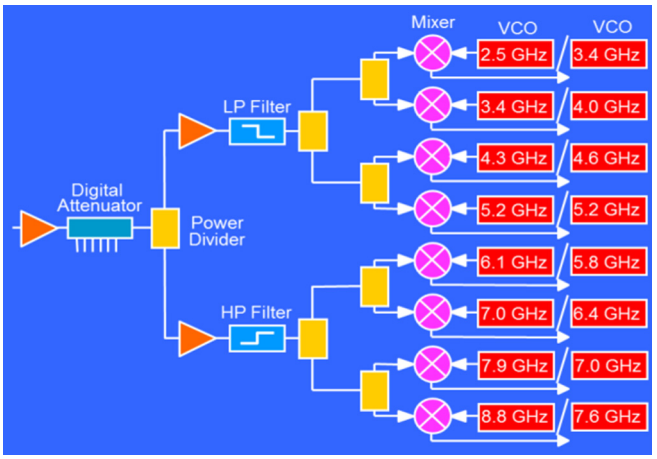

Fig. 9. Schematic diagram of the amplification and detection system.

The diagnostic should be in operation for the 2nd year of experiments on WEST. The final design review will be held in autumn 2016. The diagnostic will be assembled, aligned and tested in Korean university laboratories in the first semester of 2017. Installation on WEST is scheduled for the shutdown after the WEST first year of operation.

4. Conclusion

Microwaves diagnostics have been routinely measuring the density or temperature profiles inside the tokamak plasmas with good temporal and spatial resolution. Recent developments of imaging diagnostics based on the same techniques provide a two-dimensional images of fluctuations induced by MHD instabilities and their temporal dynamics. On WEST, the density and temperature will be measured simultaneously by ultra-fast profile reflectometry and ECEI. Reducing the reflectometry measurement time will allow us to make reconstruction with a higher angle resolution or to reconstruct faster rotation modes. ECEI will also obtain images of transient events. As MHD instabilities, such as sawteeth, could induce different evolution of density and temperature profiles, simultaneous measurement will be very useful to progress on the understanding of MHD instabilities. Confrontation of density and temperature images could also exhibit details that could help to validate or refine the MHD modelling tools.

References

[1] J. Wesson, Tokamaks, 3rd ed., Oxford University Press, Clarendon, 2004.
[2] A. Fasoli, et al., Nucl. Fusion 47 (2007) S264–S284.
[3] H. Park, et al., Rev. Sci. Instrum. 74 (2003) 4239.
[4] B.J. Tobias, et al., Rev. Sci. Instrum. 81 (2010) 10D928.
[5] I.G.J. Classen, et al., Rev. Sci. Instrum. 81 (2010) 10D929.
[6] G. Yun, et al., Rev. Sci. Instrum. 81 (2010) 10D930.
[7] H.K. Park, et al., Phys. Rev. Lett. 96 (2006) 195003.
[8] H.K. Park, et al., Phys. Rev. Lett. 96 (2006) 195004.
[9] G. Yun, et al., Phys. Rev. Lett. 107 (2011) 045004.
[10] J. Bucalossi, et al., Fusion Eng. Des. 86 (2011) 684.
[11] F. Simonet, Rev. Sci. Instrum. 56 (1985) 664.
[12] P. Varela, et al., Rev. Sci. Instrum. 66 (1995) 4942.

[13] H. Bottolier-Curtet, G. Ichtchenko, Rev. Sci. Instrum. 58 (1987) 539.
[14] F. Clairet, et al., Rev. Sci. Instrum. 72 (2001) 340.
[15] R. Sabot, et al., Rev. Sci. Instrum. 75 (2004) 2656.
[16] F. Clairet, et al., Rev. Sci. Instrum. 81 (2010) 10D903.
[17] R. Sabot, et al., Nucl. Fusion 46 (2006) S685.
[18] C. Gil, et al., Fusion Sci. Technol. 56 (2009) 1219.
[19] P. Smeulders, Nucl. Fusion 23 (1983) 529.
[20] D.J. Campbell, et al., in: Proc. 16th Conf. Plasma Physics and Controlled Fusion, vol. 2, Venice, Italy, 1989, p. 509.
[21] Y. Nagayama, Rev. Sci. Instrum. 61 (1990) 3265.
[22] V. Udintsev, Plasma Phys. Control. Fusion 47 (2005) 1111.
[23] R. Sabot, et al., Plasma Phys. Control. Fusion 48 (2006) B421.
[24] R. Guirlet, et al., Nucl. Fusion 50 (2010) 095009.
[25] T. Nicolas, et al., Phys. Plasmas 19 (2012) 112305.
[26] H. Lütjens, J.-F. Luciani, J. Comput. Phys. 229 (2010) 8130.
[27] I.H. Hutchinson, Principles of Plasmas diagnostics, Cambridge University Press, Cambridge, 2002.
[28] J.L. Ségui, et al., Rev. Sci. Instrum. 74 (2003) 4239.
[29] R.P. Hsia, et al., Rev. Sci. Instrum. 66 (1995) 834.
[30] Y. Nam, et al., Rev. Sci. Instrum. 83 (2012) 10E318.